

## Single Step Carbonization-Activation of Durian Shells for Producing Activated Carbon Monolith Electrodes

E. Taer<sup>1,\*</sup>, A. Apriwandi<sup>1</sup>, R. Taslim<sup>2</sup>, U. Malik<sup>1</sup>, Z. Usman<sup>1</sup>

<sup>1</sup> Department of Physics, University of Riau, 28293 Simpang Baru, Riau, Indonesia.

<sup>2</sup> Department of Industrial Engineering, State Islamic University of Sultan Syarif Kasim, 28293 Simpang Baru, Riau, Indonesia.

\*E-mail: [erman.taer@lecturer.unri.ac.id](mailto:erman.taer@lecturer.unri.ac.id)

Received: 8 October 2018 / Accepted: 5 December 2018 / Published: 5 January 2019

---

Four types of monolithic carbon electrodes were prepared from durian shell waste by a one-step carbonization-activation process. The activation process was performed physically at a temperature of 900 °C for 1 hour. The carbon electrodes were produced with various amounts of (i) CO<sub>2</sub> gas and (ii) steam activating agent. For both types of activation processes, the samples also varied according to their electrode particle size, i.e., (a) particles smaller than 38 microns and from to (b) 39 - 52 microns. After varying these four factors, we produced a monolithic carbon electrode with a highest specific capacitance of 130.35 F g<sup>-1</sup> with the steam activating agent and a particle size of 39-52 microns. The optimized electrochemical properties were evidenced by the physical characteristics, such as the density, specific surface area and surface morphology. The results of this study present a relatively simple process for producing supercapacitor electrodes made from durian shell waste.

---

**Keywords:** Durian shells, carbon electrode, specific capacitance, supercapacitor

### 1. INTRODUCTION

Durians are a much-loved fruit that are relatively large with a yellow fruit flesh, sweet taste and fragrant smell; hence, the durian is often referred to as the king of the fruit [1]. Durian fruit production in 2016 in Indonesia reached 995.735 tons. Seventy percent of the durian fruit is its shell, which becomes waste after the meat is taken [2]. This waste is seen in many urban areas in Indonesia, especially during the fruit season. The utilization of durian shell waste offers a solution to urban waste distribution. One way of utilizing durian shells is to convert them into activated carbon to increase their economic value [3]. The production of activated carbon from biomass materials usually includes carbonization and activation processes [4]. The carbonization process is usually carried out at a relatively low temperature from 400 to 700 °C in a controlled atmosphere environment, usually using N<sub>2</sub> or Ar gas [5]. While the

activation process can be divided into chemical and physical activation. Chemical activation using chemical activating agents such as KOH, H<sub>3</sub>PO<sub>4</sub> [6], ZnCl<sub>2</sub> [7], HNO<sub>3</sub> [8], usually occurs at low temperatures. Physical activation usually occurs at relatively higher temperatures from 800 to 1000 °C using CO<sub>2</sub> or steam [9]. The process of carbonization and activation can be conducted directly (single step) or in several steps. Single-step carbonization and activation processes can be carried out by carbonization at a certain temperature in a N<sub>2</sub> gas environment, and then, the temperature is increased to a certain temperature for the activation process in CO<sub>2</sub> gas or steam. Meanwhile, carbonization and activation with several steps involves carbonization until reaching a certain temperature, and then, the temperature is lowered to room temperature. Afterwards, the temperature is increased again to a certain temperature in an environment of CO<sub>2</sub> gas [10] or steam [11] to initiate the activation process, and then, the temperature is lowered until reaching room temperature. The single-step carbonization and activation process clearly has several benefits, such as (i) lower processing times, (ii) lower energy consumption and (iii) production cost savings.

Ong *et al.* [12] has been using durian shells as a raw material to manufacture capacitor electrodes. The process of synthesizing carbon electrodes consists of several steps: (i) carbonization, (ii) activation with ultrasonic waves and (iii) activation using microwaves. The carbon electrodes were made with the addition of an adhesive material. This method resulted in a maximum capacitance of 103.6 F g<sup>-1</sup> [12]. In this study, the carbonization and activation processes were completed in one step. Pre-carbonized samples in the form of monolith were carbonized from room temperature to 600 °C in a N<sub>2</sub> gas atmosphere; then, the furnace was programmed to a temperature of 900 °C and maintained at this temperature for 1 hour in a CO<sub>2</sub> gas atmosphere. Afterwards, the furnace was cooled to the temperature of 30 °C (room temperature). This method was also repeated for the activation process using steam. The carbon electrodes produced in this study were in the form of monoliths. It was found that the supercapacitor with the maximum capacitance using steam was 130.35 F g<sup>-1</sup>, while the activated carbon monolith (ACM) using CO<sub>2</sub> gas was 92.89 F g<sup>-1</sup>. In detail, the process of synthesizing carbon monolithic samples made from durian shells and an analysis of their physical and electrochemical properties will be discussed in the next section.

## 2. MATERIAL AND METHODS

Durian shell waste was collected from a local market in Pekanbaru, Riau province, Indonesia. The impurities of the collected samples were washed by using water flow, and then, the samples were cut into pieces with a size of 5 cm<sup>2</sup>, pounded and dried under the sun for 2 days. The samples were heated in an oven at 110 °C until the mass became constant. The pre-carbonization process was carried out at a temperature of 250 °C for 2 hours, and the samples exhibited a dark brown color. The change in the color also followed by a change in the physical characteristics of the sample, which became more fragile and produced finer particles. The pre-carbonization samples were milled using a hard grinder and ball-milling device and sieved to obtain a certain particle size. The particle sizes of the samples were sorted into two groups: (i) smaller than 38 microns and from (ii) 39 to 52 microns. Both types of samples were formed into monolith with a diameter of 2 cm using a compression machine at a pressure of 8 tons [13].

Carbonization was carried out at 600 °C in N<sub>2</sub> gas. Afterwards, the furnace temperature was increased to 900 °C and then, CO<sub>2</sub> or steam was introduced for 1 hour, followed by turning off the furnace [14]. The cooling process to room temperature was carried out in a N<sub>2</sub> gas environment. Based on these variation, the samples are labeled AC/38/CO<sub>2</sub>, AC/39-52/CO<sub>2</sub>, AC/38/H<sub>2</sub>O and AC/39-52/H<sub>2</sub>O, respectively, where AC refers to activated carbon, the number refers to particle sizes and CO<sub>2</sub> or H<sub>2</sub>O refers to physical activation agent. Next, the mass and diameter of the activated carbon monoliths were determined to calculate the density. All samples were polished to a thickness of 0.3 mm and washed in distilled water until the pH of the washing water became neutral. The physical properties of the activated carbon monoliths were characterized, including the density, thermo-gravimetric (TG), and differential thermo-gravimetric (DTG) analysis, degree of crystallinity, the surface morphology, and the element composition. The electrochemical properties were measured using cyclic voltammetry with a Physic CV UR Bio-Rad 456 instrument, which was calibrated with a Solatron 1286. The electrochemical testing was conducted in a 1 M H<sub>2</sub>SO<sub>4</sub> electrolyte solution [13]. The supercapacitor cells were made according to a procedures from previous studies [15].

### 3. RESULT AND DISCUSSION

#### 3.1. Analysis of shrinkage percentage of mass, diameter and thickness

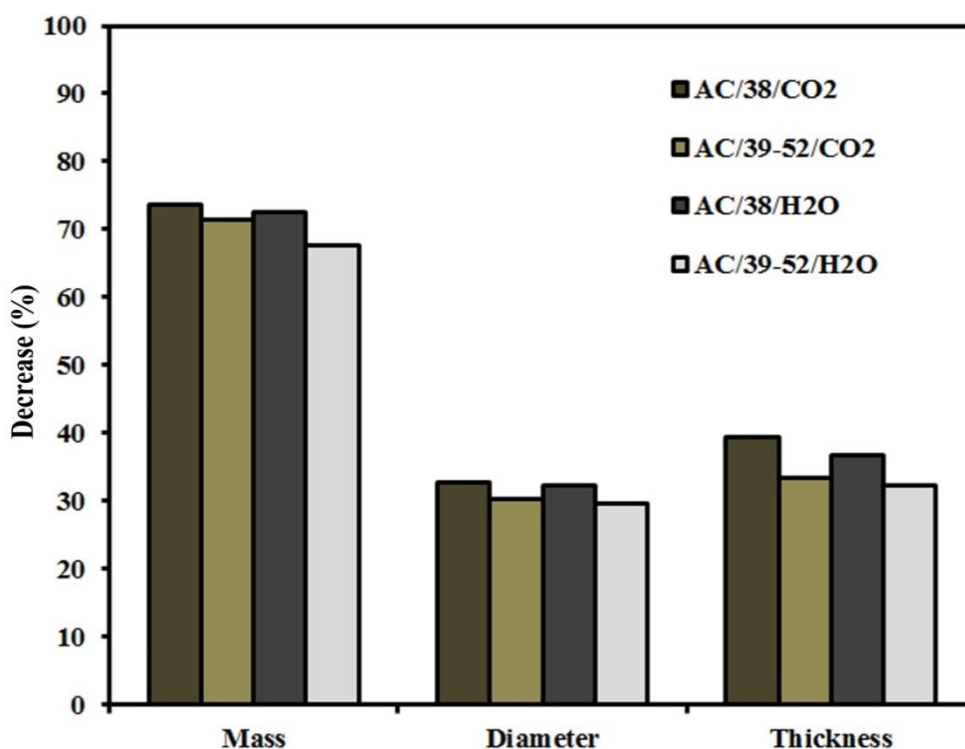
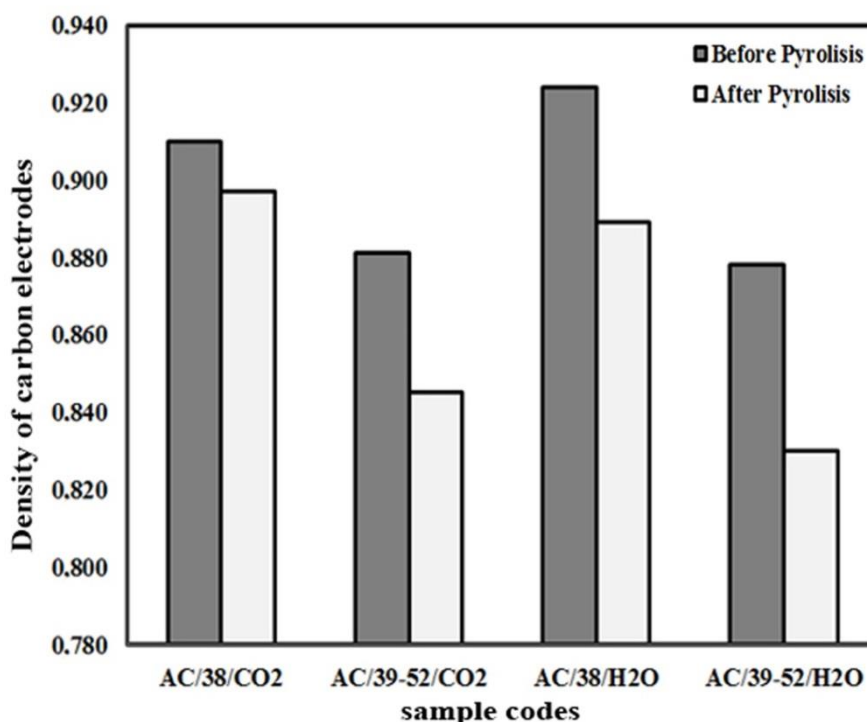


**Figure 1.** Decrease in the mass, diameter, and thickness of the activated carbon electrode after the carbonization and activation process.

Figure 1 shows the shrinkage percentage of the mass, diameter and thickness of the activated carbon monolith made from durian shells. Shrinkage percentage of mass, volume and thickness are calculated from the difference of these variables before and after pyrolysis. The mass decreased significantly. The largest mass loss occurred in the AC/38/CO<sub>2</sub> sample, while the smallest mass shrinkage was in the AC/39-52/H<sub>2</sub>O sample. The CO<sub>2</sub> activation resulted in greater mass shrinkage than steam activation. Bulk shrinkage occurred during the release of the non-carbon materials during carbonization and physical activation. The diameter and thickness also decreased, but this trend was not as significant. Smaller sample particle sizes resulted in larger mass shrinking than the bigger particle sizes. The monolith diameter did not exhibit a significant decrease, while the thickness exhibited larger shrinkage for the smaller-particle samples.

3.2. Effect carbon density data before and after the carbonization-activation process

Figure 2 shows the carbon density data before and after the carbonization-activation process. All samples exhibited a density decrease. This fact was caused by the carbonization process removing the elements other than carbon, so the density of the carbon electrode decreased, followed by the formation of pores in the carbon sample. Carbonization produces carbon that is still fragile, so it needs an activation process to produce strong carbon [16]. The particle size is the main determinant of the density value of a carbon monolith. Samples with larger particles will form larger pores between the particles, resulting in smaller bulk densities, whereas smaller particle sizes will form smaller pores between the particles, resulting in larger monolith densities. The activation process also causes a decrease in the sample density. The greatest decrease in density was found in sample AC/39-52/ H<sub>2</sub>O.



Figures 2. Density of the carbon electrodes before and after the carbonization and activation process.

The particle size affects the carbon density of the carbon sample. Non-uniform particle sizes showed larger density values, as seen in samples AC/38/CO<sub>2</sub> and AC/38/H<sub>2</sub>O. The higher densities occurred because the space between the particles as filled by the smaller particles, resulting in a greater density, whereas the uniform particle size indicated a smaller density value, as seen in the samples of AC/39-52/CO<sub>2</sub> and AC/39-52/H<sub>2</sub>O. A uniform particle size will result in a pore arrangement between the particles that produces a relatively smaller density. The density is related the porosity characteristics; the porosity of a carbon electrode influences the performance of the resulting supercapacitor cell. The relationship between density and porosity is inversely proportional; higher densities result in a smaller porosity, steam activation samples resulted in a smaller density compared to the CO<sub>2</sub> activation samples. Steam activation is capable of producing activated carbon with a higher surface area and a more uniform pore distribution than CO<sub>2</sub> activation [17].

### 3.3. Thermal characteristic of durian shell-based activated carbon

One of the methods used to study the changes in material properties after heat treatment is to use thermo-gravimetric analysis. Figure 3 shows the TG/DTG curve of the durian shell sample after the pre-carbonization process. The TG curve shows the change in the sample mass vs temperature. Significant decreases occurred in the TG curve occur from (i) 60 °C to 90 °C (as high as 4.11%) and (ii) from 200 °C to 350 °C (33.80%). The decrease in part (i) indicates the decomposition of the water content, while that in part (ii) was caused by the decomposition of complex compounds, such as hemicellulose, cellulose and lignin. The 55% hemicellulose mass degradation occurred from 200 °C to 300 °C, and the cellulose mass decomposed at from 280 °C to 390 °C [18]. The lignin decomposition occurred in the temperature region from 160 °C to 900 °C. After reaching a temperature of 350 °C, the curve still exhibited a relatively small mass decrease. The mass decrease above 350 °C was due to the unfinished cellulose and lignin decomposition. The DTG curve shows two peaks, in the region from 60 °C to 90 °C and at 305.3 °C. This peak indicates that at these two points, there is a greater reduction in the mass per unit of time. The first peak occurs because of the decomposition of the water content in the sample material, and the second peak occurs at a temperature of 305.3 °C reaches 0.410 mg min<sup>-1</sup>. This temperature is the intersection for the decomposition of all complex compounds that comprise the sample materials, such as hemicellulose, cellulose and lignin [19]. This analysis is very compatible with the TG curve, which also exhibited a significant decrease. It can be concluded that a temperature of 305.3 °C is the optimum temperature for the decomposition process of durian shells. The temperature of 305.3 °C was then selected as the resistance temperature for the carbonization process with the durian shell material. Other studies have presented the decomposition of cellulose and hemicellulose within the same temperature range, such as for date palms [20] and rubber seed [21]. The decomposition of hemicellulose and cellulose within date palms occurred in the temperature range from 250-375 °C, and the decomposition in the rubber seeds occurred within the temperature range from 273-385 °C. We can conclude that the TG data for durian shells are similar to those of other biomass materials such as date palms and rubber seeds.

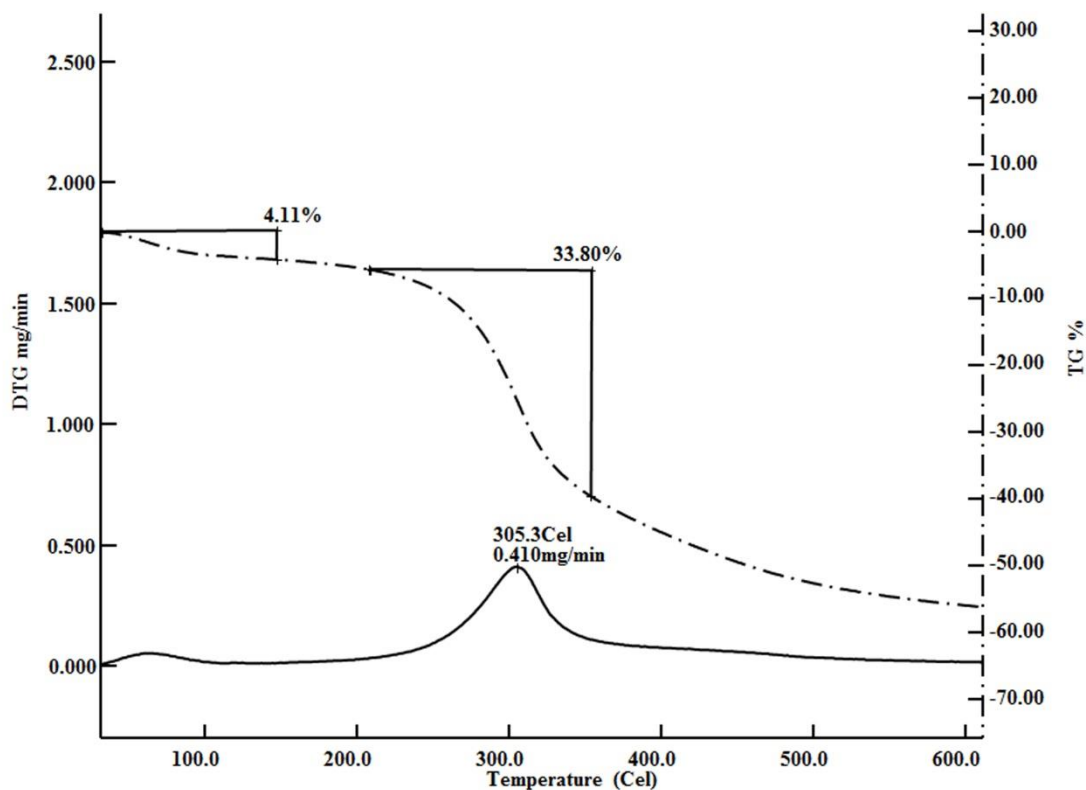
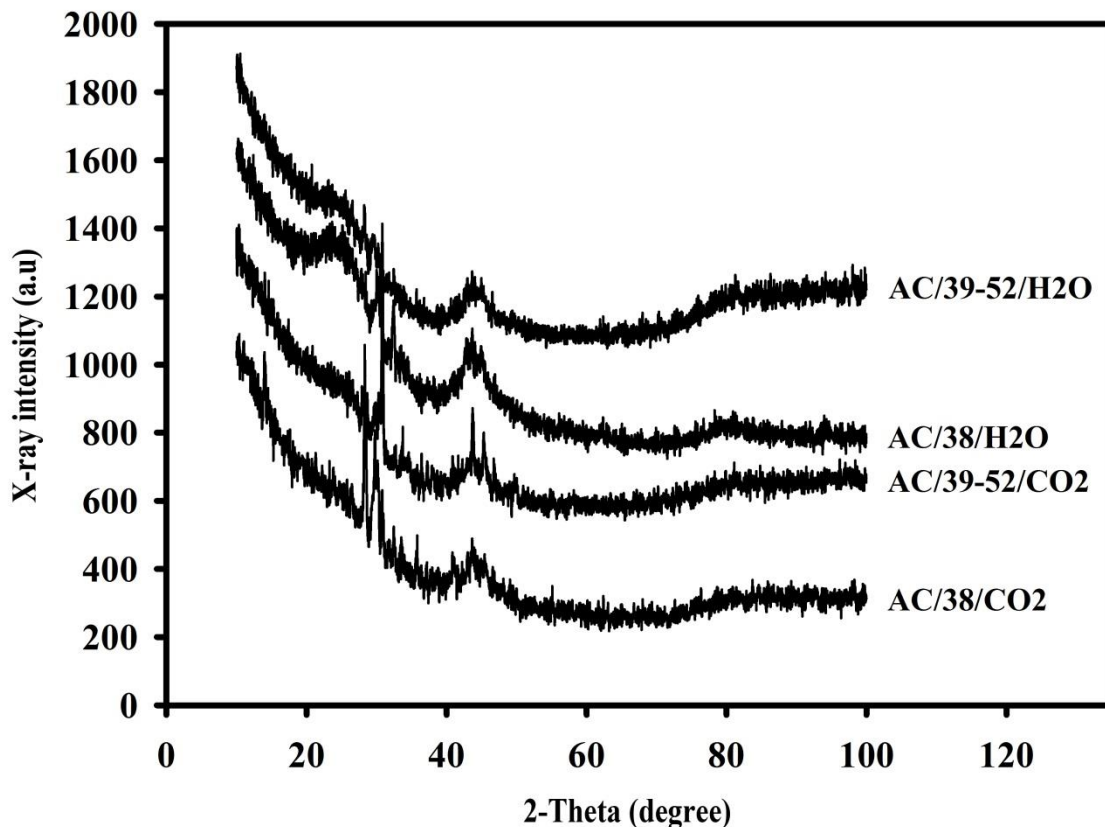


Figure 3. TG and DTG curves for the precarbonized sample

### 3.4. Structural analysis using X-Ray Diffraction

The X-ray diffraction curve of activated carbon from the durian shells is shown in Figure 4. Two broadening peaks at 2 theta values of 24 and 44 in the X-ray diffraction curves show the presence of carbon materials within amorphous structures [22]. The  $2\theta$  diffraction angles in the reflection planes of 002 and 100 for the AC/38/CO<sub>2</sub> sample were 25.382° and 45.045°, 25.215° and 44.260° for the AC/39-52/CO<sub>2</sub> sample, 25.359° and 44.583° for the AC/38/H<sub>2</sub>O sample, and 22.715° and 44.830° for the AC/39-52 / H<sub>2</sub>O sample, respectively. These data show that the samples exhibited good peaks for carbon materials [22].

Figure 4 shows the differences in the peak heights while varying the particle sizes. The carbon samples with uniform particle sizes (AC/39-52/CO<sub>2</sub>) showed clearer and wider peaks in the reflection plane of 002 with an intensity of 328.37 nm, whereas the carbon with non-uniform particle sizes only exhibited a diffraction intensity as high as 190.66 nm. These results indicate that samples with uniform particle sizes have better scattering-plane regularity compared to particles with non-uniform sizes. The different activation environments (CO<sub>2</sub> and steam) also exhibited differences in the X-ray diffraction curves. The activated carbon sample with CO<sub>2</sub> gas (AC/39-52/CO<sub>2</sub>) had the highest peak intensity at 328.37 nm with a half-width peak value of 9.6059 nm. The activated carbon sample with steam (AC/39-52/H<sub>2</sub>O) had the highest peak intensity at 190.66 nm with a half-peak width of 10.007 nm.



**Figures 4.** The XRD patterns for the durian shell-based activated carbon.

These data indicate that the regularity of the scattering plane of the carbon samples from durian shells using CO<sub>2</sub> activation was better than that using steam. Deraman *et al.* [23] showed that X-ray diffraction data can be used to determine the surface area of carbon. The relation between the surface area and stack height ( $L_c$ ) can be obtained by following formula:

$$SSA_{xrd} = 2/(\rho_{xrd}L_c)$$

where  $\rho_{xrd}$  is the XRD density, which is evaluated using the following equation:

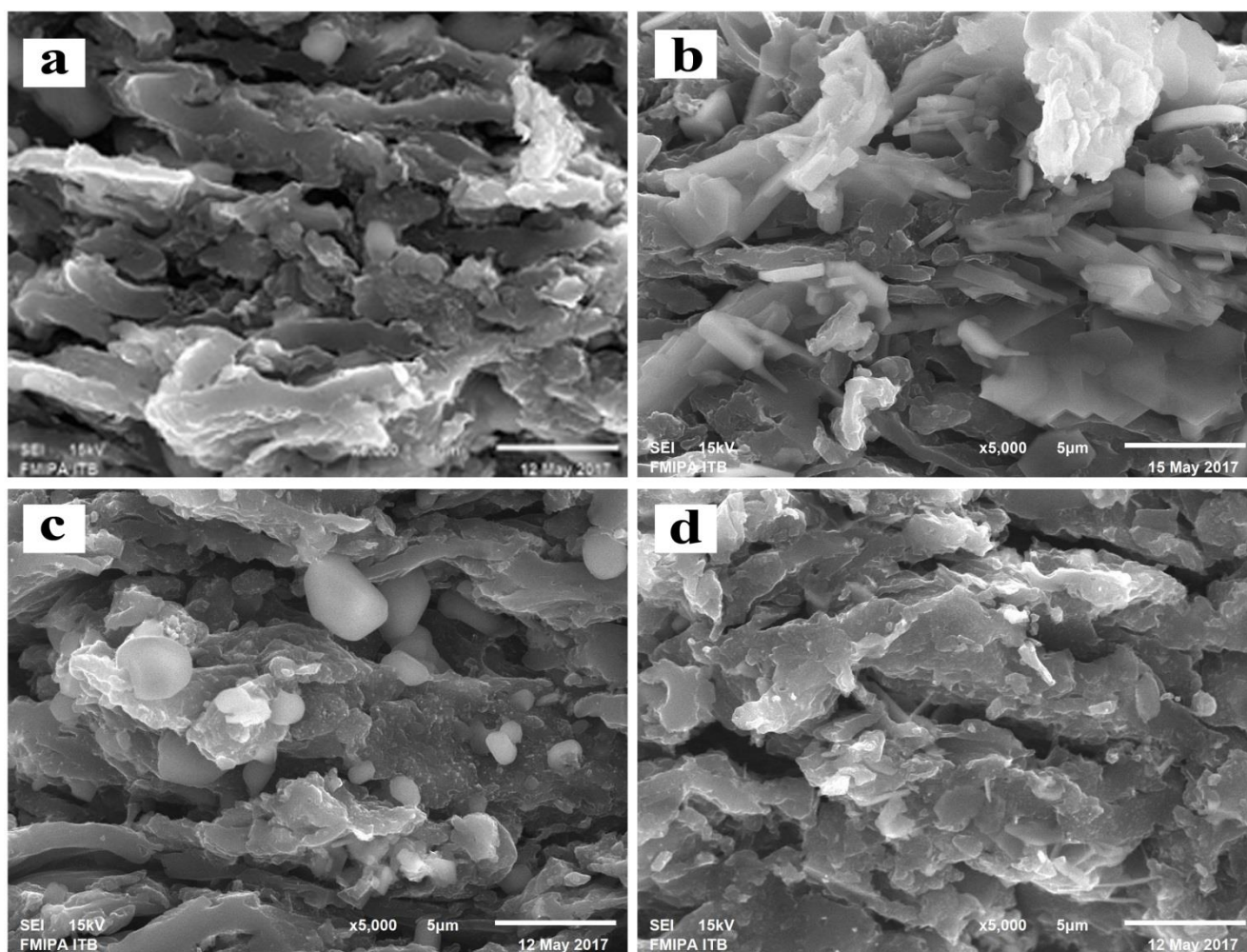
$$\rho_{xrd} = (d_{002}(\text{graphite})/d_{002}(\text{sample})) \rho(\text{graphite})$$

where  $d_{002}(\text{graphite})$  and  $\rho(\text{graphite})$  are 0.33354 nm and 2.268 g cm<sup>-3</sup>. The surface area of the activated carbon affected the specific capacitance value of the supercapacitor. Based on this formula, the optimum surface area in this study was found to be 1838,47 cm<sup>2</sup> g<sup>-1</sup>.

### 3.5. Scanning electron microscopy (SEM) observation

The SEM micrographs in Figures 5a, b, c and d represent the AC/38/CO<sub>2</sub>, AC/38/ H<sub>2</sub>O, AC/39-52/CO<sub>2</sub>, AC/39-52/H<sub>2</sub>O samples, respectively. Figures 5a and 5b show that the morphology of the electrode at the cross-sectional area was dominated by particles with a relatively small, finer size, and large spaces (macro pores) were observed between the particles. The size of the spaces formed ranged from 0.40 μm to 0.69 μm with particle sizes ranging from 1.28 μm to 6.28 μm. Figures 5c and 5d show that the SEM micrograph was dominated by larger particles, and the visible presence of larger macro

pores is indicated by the darker colors. These macro pores indicated that the samples with uniformly sized particles (39-52  $\mu\text{m}$ ) had pores between the larger particles ranging from 0.48  $\mu\text{m}$  to 2.66  $\mu\text{m}$  with particles sizes ranging from 1.48  $\mu\text{m}$  to 6.89  $\mu\text{m}$ . Based on the variations in the activation process, different sample morphologies were observed. Samples with  $\text{H}_2\text{O}$  activation had pore sizes between the particles ranging from 0.57  $\mu\text{m}$  to 2.66  $\mu\text{m}$ , while the pore sizes between the particles for the  $\text{CO}_2$  activation sample ranged from 0.4  $\mu\text{m}$  to 1.4  $\mu\text{m}$ . These data suggest that the pores between the particles generated through  $\text{CO}_2$  gas activation were smaller than those observed in the steam samples [24]. The activated samples using steam exhibited flat pore shapes, appearing similar to a labyrinth [25]. The presence of these flat pores indicated that samples with steam activation had good porosity properties.



**Figures 5.** SEM micrograph at magnification of 5000 for different samples: (a) AC/38/ $\text{CO}_2$ , (b) AC/38/ $\text{H}_2\text{O}$ , (c) AC/39-52/ $\text{CO}_2$ , and (d) AC/39-52/ $\text{H}_2\text{O}$

### 3.6. EDX analysis

An energy dispersive X-ray (EDX) analysis was conducted to determine the compositions of the carbon electrodes. The elements of the durian shell-based activated carbon samples are shown in Table 1. Based on the data in Table 1, the electrode consisted of carbon (C), oxygen (O), magnesium (Mg),

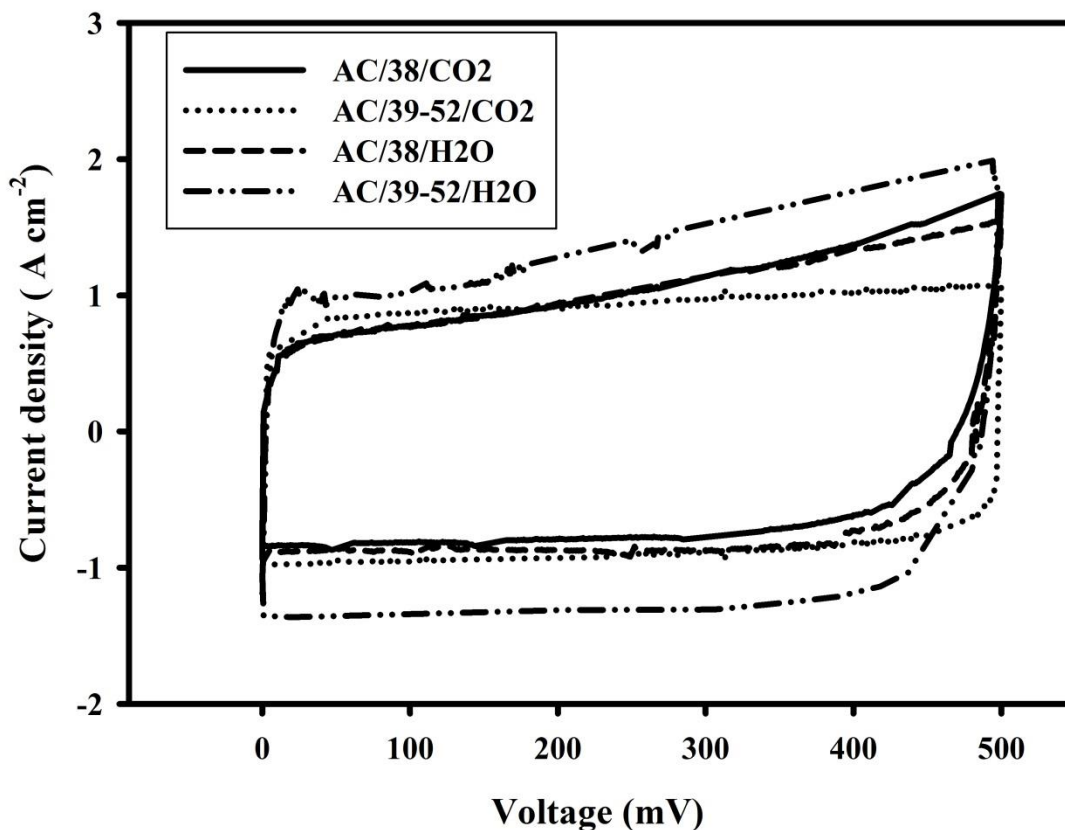
silicon (Si), phosphorus (P), and potassium (K). Carbon was the dominant element with a range from 84% to 91%. These results prove that the sample predominantly contained carbon as desired. The oxygen element was also dominant in the sample; oxygen was present from the activation agent of CO<sub>2</sub> and steam. The presence of potassium, with the largest amount after carbon, indicated that the composition of the durian shell was also mostly dominated by potassium. Based on the EDX analysis, the highest quantity of carbon was found in the AC/39-52/H<sub>2</sub>O sample with 90.69%, while the lowest quantity of carbon was observed in the AC/38/CO<sub>2</sub> sample. The different particle sizes in the samples resulted in different levels of carbon content. The uniform particle size (39 μm to 52 μm) yielded a higher quantity of carbon than the non-uniform particle size (<38 μm). This larger carbon quantity in the uniform samples was due to the ability of the activating gas flow to easily reach all parts of the electrode. This result reinforces the preceding analysis in which the uniform particle sizes yielded more and better carbon within the activated carbon monolith sample. The differences between the CO<sub>2</sub> and steam activators did not result in significant difference in the carbon content in the samples. The activated carbon with uniformly sized particles activated using CO<sub>2</sub> and steam exhibited nearly the same carbon quantity. The carbon purity data results are similar to those from other studies regarding bamboo waste [26] and banana stem [27]. The activated carbon from bamboo waste with steam activation had a carbon purity of 81.18%, and the activated carbon from date palms with CO<sub>2</sub> activation had a carbon purity of 77.83%.

**Table 1.** The quantity of the elements in the durian shell-based activated carbon

Elements	The quantity of the compound element for durian shells based activated carbon			
	AC/38/CO <sub>2</sub> (%)	AC/39-52/CO <sub>2</sub> (%)	AC/38/H <sub>2</sub> O (%)	AC/39-52/H <sub>2</sub> O (%)
C	84.5030	90.2747	86.9721	90.6906
O	3.7482	3.3611	5.0877	2.3869
Mg	0.7459	0.6336	0.9256	0.5147
Si	0.3991	0	0.2039	0.3846
P	0.6958	0.5329	0.5398	0.5017
K	9.9080	5.1977	6.2708	5.5214

### 3.7. Electrochemical performance of activated carbon based on durian shells

Cyclic voltammetry (CV) is a method used to obtain the relationship between the current density of charging-discharging vs the potential in a supercapacitor cell. The CV data were used to calculate the specific capacitance of the carbon electrodes. Figure 6 shows the potential vs current curves for the different supercapacitor cells. The largest current-potential area was found in the AC/39-52/H<sub>2</sub>O sample, while the smallest curve area occurred in the cells of the AC/38/CO<sub>2</sub> electrodes. The activation process using steam resulted in samples with a higher surface area compared to samples activated using CO<sub>2</sub> gas. The steam activation process produced samples dominated by mesopores, and CO<sub>2</sub> activation produced samples dominated by microspores [17].



Figures 6. CV curves for different supercapacitor cells

Therefore, the electrolyte ions were able to more easily diffuse into the meso and micropores of the electrodes. The larger current and voltage area corresponded to a higher specific capacitance. Based on the calculation using formula (ii), it was found that the highest specific capacitance in the AC/39-52/H<sub>2</sub>O sample was 130.35 F g<sup>-1</sup>, while the lowest specific capacitance was 90.04 F g<sup>-1</sup> for the AC/38/CO<sub>2</sub> sample. The resulting capacitive properties of the supercapacitor cell are consistent with the density and porosity characteristics that were previously discussed. The specific capacitance value of the active carbon electrodes at a scan rate of 1 mV s<sup>-1</sup>, is shown in Table 2. Figure 7 shows the specific capacitance of the supercapacitor cell vs the scan rate. The specific capacitance decreases as the rate of scanning increases. The decrease in the specific capacitance is due to the fact that at a larger scan rate, the electrolyte ions do not have sufficient time to diffuse into the carbon pores, resulting in a smaller specific capacitance.

Table 2. Specific capacitance of the supercapacitor cells with different activated carbon electrodes made from durian shells.

Sample codes	Mass (g)	thickness (mm)	Specific capacity (F g <sup>-1</sup> )
AC/38/CO <sub>2</sub>	0.020	0.19	90.04
AC/39-52/CO <sub>2</sub>	0.019	0.17	92.89
AC/38/H <sub>2</sub> O	0.017	0.17	112.12
AC/39-52/H <sub>2</sub> O	0.020	0.18	130.35

The series of studies and analyses indicate that the single-step carbonization and activation method was successfully developed. Using durian shells as a raw material to produce electrode supercapacitors resulted in electrodes with good physical and electrochemical properties. The physical properties, such as the density, stack height ( $L_c$ ) and specific capacitance, of the best samples were  $0.830 \text{ g cm}^{-3}$ ,  $6.9977 \text{ \AA}$ , and  $130.35 \text{ F g}^{-1}$ , respectively. The surface morphological studies showed that the surface of the sample was dominated by open macro pores between the electrode particles. The obtained capacitive properties were relatively better than those reported by Ong *et al.* [12] using the same material. In addition, the resulting capacitive electrode is almost the same as the other capacitive electrode with a different biomass such as shown on Table 3. Based on this study, the single-step carbonization and activation process can be recommended as an alternative method for producing carbon monolith electrodes for supercapacitor applications.

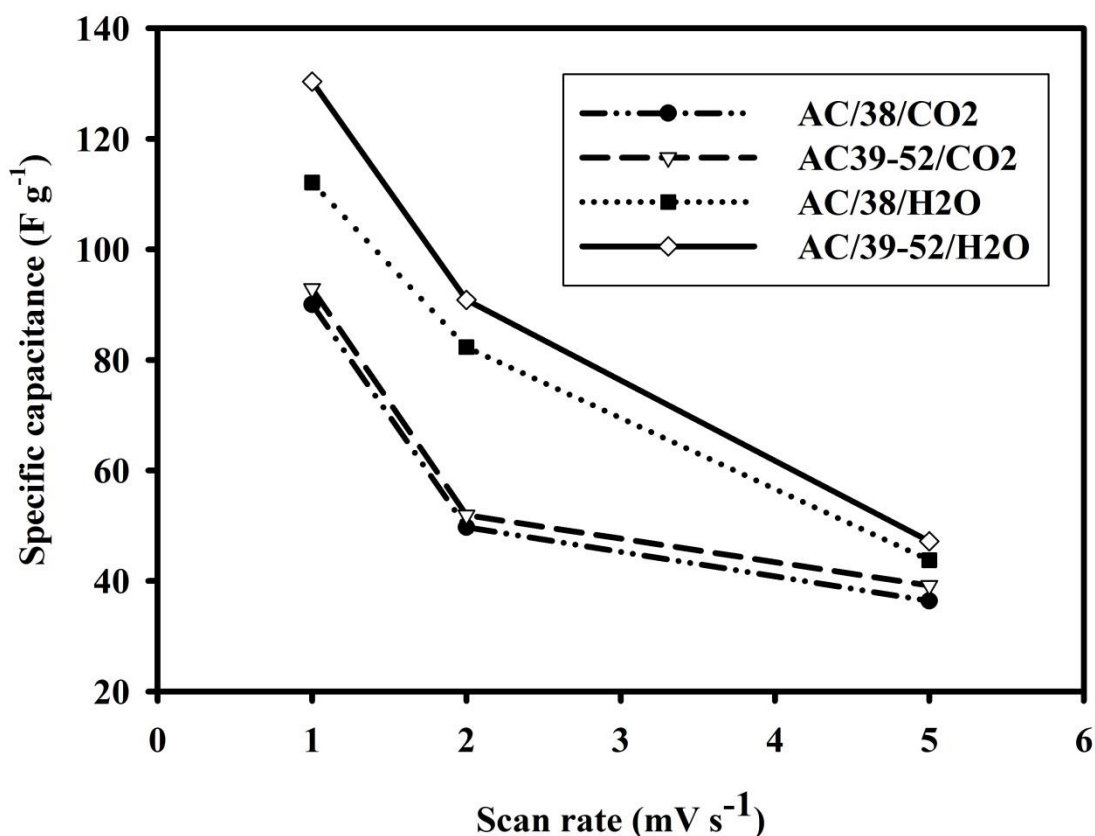


Figure 7. Specific capacitance ( $\text{F g}^{-1}$ ) vs the scanning rate ( $\text{mV s}^{-1}$ ) for different supercapacitor cells.

Table 3. Specific capacitance for other biomass

Biomass	Specific capacitance	References
Rubber wood sawdust	50.65	[28]
Cow dung	124	[29]
Corn stalk	140	[30]
Olive residues	193	[31]
Cattail	126	[32]
oil palm empty fruit bunches	117.7	[33]
Durian shell	130.35	Present study

#### 4. CONCLUSION

A single-step carbonization and activation method for producing carbon electrodes from biomass waste was successfully demonstrated. This single-step method clearly reduces the time required for processing carbon electrodes and certainly reduces the production costs. The activated carbon monolith from durian shell waste produced using the single-step method demonstrated good physical and electrochemical properties. The CO<sub>2</sub> and steam activation resulted in slightly different physical and electrochemical properties, from which the steam activation produced carbon electrodes with better pore and capacitive properties. The optimum specific capacitance using steam activation was 130.35 F g<sup>-1</sup>.

#### ACKNOWLEDGEMENTS

We acknowledge research funding support from DRPM KEMENRISTEK-DIKTI under grant *Penelitian Unggulan Perguruan Tinggi* (PUPT) No. 540/UN/19.5.1.3/PP/2017.

#### References

1. T. W. Afrilia, Nurbani, *Prossiding Seminar Nasional, Masy Biodiv Indon.*, 3 (2007) 132.
2. Badan Pusat Statistik, *Produksi Buah di Indonesia*. (2016) Jakarta.
3. C. C. Thio, M.M. Magdalena, S. Jaka, S. Yohanes, I. Suryadi, *The Taiwan Institute of Chemical Engineers*, 40 (2009) 457.
4. G. Dobele, T. Dizhbite, M. V. Gil, A. Volperts, T. A. Centeno, *Bio mass and bioenergy*, 46 (2012) 145.
5. Z. Yue, J. Economy, *the textile intitute*. (2017) Woodhead Publishing.
6. A. Elmouwahidi, E. Bailón-García, Agustín, F. Pérez-Cadenas, Francisco J. Maldonado-Hódar, F. Carrasco-Marín, *Electrochimica Acta*, 229 (2017) 219.
7. W. Changshui, L. Tingzhi, *Alloys and Compounds*, 69 (2017) 42.
8. S. Tao, X. Jun, S. Lai-hong, *New Carbon Materials*, 30 (2015) 156.
9. M. A. Adekunle, N. A. Farid, *Renewable and Sustainable Energy Reviews*, 52 (2015) 1282.
10. S. Min, J. Baosheng, X. Rui, Y. Li, W. Yimin, Z. Zhaoping, H. Yaji, *Bio mass and bioenergy*, 48 (2013) 250.
11. M. Plaza-Recobert, G. Trautweina, M. Perez-Cadenas, J. Alcaniz-Monge, *Microporous and Mesoporous Materials*, 243 (2017) 28.
12. L. K. Ong, A. Kurniawana, A. C. Suwandia, C. X. Lin, X. S. Zhao, S. Ismadji, *Progress in Natural Science: Materials International*, 6 (2012) 624.
13. R. Farma, M. Deraman, R. Omar, Awitdrus, M. M. Ishak, E. Taer, I. A. Talib, *AIP Conf. Proc.*, 1415 (2011) 180.
14. E. Taer, Apriwandi, Yusriwandi, W. S. Mustika, Zulkifli, R. Taslim, Sugianto, B. Kurniasih, Agustino, P. Dewi, *AIP Conf. Proc.*, 1927 (2018) 030036-1.
15. E. Taer, M. Deraman, R. Taslim, Iwantono, *AIP Conf. Proc.*, 1554 (2013) 33.
16. A. Imran, M. Asim, A. K. Tabrez, *Environmental Management*, 113 (2012) 170.
17. Y. Z. Zhang, Z. J. Xing, Z. K. Duan, M. Li, Y. Wang, *Applied Surface Science*, 315 (2014) 279.
18. M. Brebu, C. Vasile, *Cellulose Chem. Technol.*, 44 (2010) 353.
19. E. Taer, A. Afrianda, Apriwandi, R. Taslim, A. Agustino, Awitdrus, R. Farma, *Int. J. Electrochem. Sci.*, 13 (2018) 10688.
20. M. Shoaib, H. M. Al-Swaidan, *Biomass and bio energy*, 73 (2015) 124.
21. S. Kang, J. Jianchun, *Biomass and bioenergy*, 34 (2010) 539.

22. E. Taer, P. Dewi, Sugianto, R. Syech, R. Taslim, Salomo, Y. Susanti, A. Purnama, Apriwandi, Agustino, R. N. Setiadi, *AIP Conf. Proc.*, 1927 (2018) 030026-1.
23. M. Deraman, R. Daik, S. Soltaninejad, N. S. M. Nor, Awitdrus, R. Farma, N. F. Mamat, N. H. Basri, M. A. R. Othman, *Adv Materials Research*, 1108 (2015) 1.
24. O. Martin, B. Lars, S. Irena, K. Nicole, L. Matthias, K. Stefan, *Carbon*, 56 (2013) 139.
25. Z. Liling, H. Da, H. Nantao, Y. Chao, L. Ming, W. Hao, Y. Zhi, S. Yanjie, Z. Yafei, *J. Power Sources*, 342 (2017) 1.
26. M. Yu, Y. Y. Han, J. Li, L. J. Wang, *Chemical Engineering Journal*, 317 (2017) 493.
27. E. Taer, R. Taslim, W. S. Mustika, B. Kurniasih, Agustino, A. Afrianda, Apriwandi, *Int. J. Electrochem. Sci.*, 13 (2018) 8428.
28. E. Taer, B. Kurniasih, F. P. Sari, Zulkifli, R. Taslim, Sugianto, A. Purnama, Apriwandi, Y. Susanti, *AIP Conf. Proc.*, 1927 (2018) 030006-1
29. D. Bhattacharjya, J-S. Yu, *J. Power Sources*, 262 (2014) 224.
30. K. Yu, H. Zhu, H. Qi, C. Liang, *Diamond & Related Mater.*, 88 (2018) 18.
31. A. Elmouwahidi, E. Bailon-Garcia, A. F. Perez-Cadenas, F. J. Maldonado-Hodar, F. Carrasco-Marin, *Electrochem. Acta*, 229 (2018) 219.
32. M. Yu, Y. Han, J. Li, L. Wang, *Chemical Engineering Journal*, 317 (2017) 493.
33. R. Farma, M. Deraman, R. Omar, Awitdrus, M. M. Ishak, E. Taer, I. A. Talib, *AIP Conf. Proc.*, 1415 (2011) 180.

© 2019 The Authors. Published by ESG ([www.electrochemsci.org](http://www.electrochemsci.org)). This article is an open access article distributed under the terms and conditions of the Creative Commons Attribution license (<http://creativecommons.org/licenses/by/4.0/>).